SCH28080, a K^+-Competitive Inhibitor of the Gastric H,K-ATPase, Binds Near the M5−6 Luminal Loop, Preventing K^+ Access to the Ion Binding Domain†

O. Vagin, S. Denevich, K. Munson, and G. Sachs*

Department of Physiology and Medicine, University of California at Los Angeles and Veteran Administration of Greater Los Angeles Health System, Los Angeles, California 90073

Received April 4, 2002; Revised Manuscript Received July 26, 2002

ABSTRACT: Inhibition of the gastric H,K-ATPase by the imidazo[1,2-α]pyridine, SCH28080, is strictly competitive with respect to K^+ or its surrogate, NH_4^+. The inhibitory kinetics [V_{max}, $K_{m,app}(NH_4^+)$, K_i(SCH28080), and competitive, mixed, or noncompetitive] of mutants can define the inhibitor binding domain and the route to the ion binding region within M4−6. While mutations Y799F, Y802F, I803L, S806N, V807I (M5), L811V (M5−6), Y928H (M8), and Q905N (M7−8) had no effect on inhibitor kinetics, mutations P798C, Y802L, P810A, P810G, C813A or -S, I814V or -F, F818C, T823V (M5, M5−6, and M6), E914Q, F917Y, G918E, T929L, and F932L (M7−8 and M8) reduced the affinity for SCH28080 up to 10-fold without affecting the nature of the kinetics. In contrast, the L809F substitution in the loop between M5 and M6 resulted in an ∼100-fold decrease in inhibitor affinity, and substitutions L809V, I816L, Y925F, and M937V (M5−6, M6, and M8) reduced the inhibitor affinity by 10-fold, all resulting in noncompetitive kinetics. The mutants L811F, Y922I, and I940A also reduced the inhibitor affinity up to 10-fold but resulted in mixed inhibition. The mutations I819L, Q923V, and Y925A also gave mixed inhibition but without a change in inhibitor affinity. These data, and the 9-fold loss of SCH28080 affinity in the C813T mutant, suggest that the binding domain for SCH28080 contains the surface between L809 in the M5−6 loop and C813 at the luminal end of M6, approximately two helical turns down from the ion binding region, where it blocks the normal ion access pathway. On the basis of a model of the Ca-ATPase in the E_2 conformation (PDB entry 1kju), the mutants that change the nature of the kinetics are arranged on one side of M8 and on the adjacent side of the M5−6 loop and M6 itself. This suggests that mutations in this region modify the enzyme structure so that K^+ can access the ion binding domain even with SCH28080 bound.

The gastric H,K-ATPase and the Na,K-ATPases belong to the P_2 family of transport ATPases. The enzymes go through a cycle of phosphorylation and dephosphorylation coupled to ion transport, protons or hydronium in exchange for potassium (H,K-ATPase) and sodium in exchange for potassium (Na,K-ATPase). Both enzymes are heterodimers, consisting of a catalytic α and an accessory β subunit (*1*−*6*). The α subunits of H,K-ATPase and Na,K-ATPase have 10 transmembrane segments (M1−10)[1] like all P_2-type ATPases, and the β subunit has a single transmembrane segment. The α subunits are 75% homologous, and the β subunit of the H,K-ATPase is 35% homologous with the β-2 subunit of the Na,K-ATPase. Both enzymes are K^+ countertransport pumps, the ATPase being stimulated by luminal K^+.

The catalytic steps are similar; however, the Na pump exchanges three Na^+ for two K^+, whereas the H,K-ATPase exchanges two H^+ for two K^+ at neutral pH (*7*). The two enzymes differ also in their inhibitor sensitivity. Ouabain inhibits the Na,K-ATPase but not the H,K-ATPase, and conversely, the imidazo[1,2-α]pyridine, SCH28080, inhibits the H,K-ATPase but not the Na,K-ATPase. Both inhibitors gain access to their binding sites from the exoplasmic surface and stabilize the E_2 conformation (*8*−*11*). SCH28080 is strictly K^+ competitive and is active in its protonated form (*10*), and the Na,K ATPase inhibitior ouabain is also K^+-competitive (*12*). Knowledge of the amino acids that affect inhibition by SCH28080 should provide insight into the regions of the membrane domain of the H,K-ATPase responsible for the selectivity of SCH28080 and for the competition between K^+ and SCH28080 as well as identifying a region whose conformation changes during the E_1 to E_2 transition.

The only high-resolution crystal structure of any P_2-type ATPases available to date is that of the SERCA-ATPase at 2.6 Å (*13*) crystallized in the E_1·2Ca state. In addition, a lower-resolution model (6.0 Å resolution) derived from electron diffraction data recently was published for the E_2 form of the Ca-ATPase (PDB entry 1kju). In this report, we have used the 1kju structure as a template upon which to map the corresponding residues of the H,K-ATPase based

† Supported in part by NIH Grants DK46917, -53462, -41301, and -17294.

* To whom correspondence should be addressed: VAGLAHS/West LA, Building 113, Room 324, 11301 Wilshire Blvd., Los Angeles, CA 90073. Phone: (310) 268-4672. Fax: (310) 312-9478. E-mail: gsachs@ucla.edu.

[1] Abbreviations: G1, hog gastric vesicles; K_i(SCH28080), apparent affinity for the inhibitor; $K_{m,app}(NH_4^+)$, apparent affinity for the cation (NH_4^+); M*X*−*Y*, exoplasmic loop; M, transmembrane helix; P_i, inorganic phosphate; PIPES, piperazine-*N*,*N*′-bis(2-ethanesulfonic acid); SCH28080, 3-(cyanomethyl)-2-methyl-8-(phenylmethoxy)imidazo[1,2-α]pyridine; SE, standard error; SERCA-ATPase, sarcoplasmic reticulum Ca-ATPase; V_{max}, maximal specific activity; wt, wild-type.

10.1021/bi025921w CCC: $22.00
Published on Web 09/26/2002

on amino acid sequence alignments. In the absence of a high-resolution crystal structure for the gastric H,K-ATPase, SCH28080 inhibitor kinetics provide a means for testing the validity of adopting the Ca-ATPase structures as reasonable backbone templates for the H,K-ATPase and suggest where modification of the backbone position of specific residues may be necessary to account for observations at odds with those derived from the Ca-ATPase structure. Using SCH28080 as a probe also defines a luminally accessible vestibule within the H,K-ATPase membrane domain, the conformation of which is sensitive to the presence of K within the ion transport site.

Mutagenesis of the gastric H,K-ATPase has shown that residues aligned with those binding Ca in the Ca-ATPase (Glu343, Glu795, Glu820, Asp824, and Glu936) and Lys791 also form part of the ion transport region but are not directly involved in SCH28080 binding (*14*). This interpretation was particularly supported by a mutation of E936 to D which changed the mechanism of inhibition to noncompetitive with only a 2-fold decrease in ion and SCH28080 affinities. Here we describe several additional mutants giving noncompetitive inhibition, confirming that the inhibitor and ion can bind simultaneously in these cases and that therefore their sites are physically distinct.

The results of previous mutations that reduced SCH28080 affinity 5−10-fold, namely, mutations of Cys813 (*15*) and Ile816 in M6 (*16*) and Met334 in M4 (*17*), show that the inhibitor binds closer to the luminal surface of the pump than the counterion. A binding cavity with general dimensions that are sufficient for SCH28080 exists at the luminal end of the M6 membrane helix as shown by labeling of C813 by omeprazole, a substituted thiophilic pryidyl methylsulfinyl benzimidazole.

Since the ion transport site and inhibitor site are apparently separate (*14*, *15*), it is likely the inhibitor blocks ion access and the residues affecting SCH28080 affinity would potentially lie in or near the luminal ion entry path distal to the ion site. This path would be closed in the E_1 and E_2K conformations, to which SCH28080 does not bind. Since side chains from M4−6 and perhaps M8 form the ion transport domain, SCH28080 must block the ion pathway between these transmembrane helices.

Scanning site-directed mutagenesis was performed on residues of the inner surface of membrane helices (M5, -6, and -8), as predicted from the model of the Ca-ATPase in the E_2 conformation (PDB entry 1kju). These changes, starting from the ion binding region and moving toward the luminal surface of the enzyme, showed that some residues not only were implicated in inhibitor affinity but also were involved in the nature of the inhibition, since their substitution changed the inhibition from competitive to mixed or noncompetitive. It appears that several mutations of the residues on adjacent sides of M8 and M6 and in the M5−6 loop provide a structure that allows K^+ access to the ion transport site in the presence of bound SCH28080, resulting in noncompetitive or mixed kinetics.

MATERIALS AND METHODS

Site-Directed Mutagenesis, Transfection of HEK293 Cells, and Selection of Stable Cell Lines. The cDNA encoding the rabbit H,K-ATPase α subunit (*18*) (GenBank accession number X64694) was inserted into the multiple cloning site of the mammalian expression vector pcDNA 3.1(Zeo) (Invitrogen, Carlsbad, CA) containing the eukaryotic selection marker Zeocin (Invitrogen) to form pcDNA3.1(Zeo)-H,K-α. The cDNA encoding the rabbit H,K-ATPase β subunit (*19*) (GenBank accession number M35544) was inserted into the multiple cloning site of the mammalian expression vector pcDNA 3(G418) (Invitrogen) containing the eukaryotic selection marker G418 for neomycin resistance [pcDNA3(G418)-H,K-β].

Mutants were generated by using the Quickchange mutagenesis kit (Stratagene, La Jolla, CA). Targeted amino acid positions in M5, -6, and -8 or in the M5−6 loop were substituted either with residues present in Na,K-ATPase or with residues selected to manipulate the chemical character of the side chain. The list of mutations is presented in Table 1.

Human embryonic kidney cells (HEK293-ATCC CRL 1573) were transfected with pcDNA3(G418)-H,K-β as previously reported (*20*), and a stable cell line was selected by adding, 60 h after transfection, the eukaryotic selection marker G418 at a concentration of 0.75 mg of G418/mL of medium. This concentration of G418 was maintained until single colonies appeared. The colonies were isolated, expanded, and grown in the presence of 0.25 mg of G418/mL of medium. The stable expression of the H,K-ATPase β subunit was confirmed by Western blot analysis using a monoclonal antibody against the H,K-ATPase β subunit, as described below. The clone with the highest level of expression of the H,K-ATPase β subunit (*17*) was then subjected to a second transfection with pcDNA3.1(Zeo)-H,K-α containing either wt or mutant H,K-ATPase α subunit cDNAs. By addition of the second eukaryotic selection marker Zeocin at a concentration of 0.4 mg/mL of medium in addition to the maintenance concentration of G418 of 0.25 mg/mL of medium, 15−20 stable cell lines expressing H,K-ATPase α as well as β subunits were selected. Two clones with the best ratio of expressed H,K-ATPase to total protein were expanded for isolation of membranes. The maintenance concentration for Zeocin was 0.1 mg/mL of medium.

Preparation of Crude Membranes. Cell layers from stable cell lines were grown to confluence and left in the flasks for an additional 2−3 days until the cell culture became overgrown (cells growing on the top of the cells attached to the bottom of the flask) and the medium started to turn yellow. The medium was changed, and the cells were left in the same flasks for an additional 2 days. The cells were resuspended in sodium free buffer A [10 mM PIPES/Tris, 2 mM EGTA, and 2 mM EDTA (pH 7.0) containing 250 mM sucrose]. The cell suspension was homogenized with a tight Dounce homogenizer (Wheaton, Millville, NY). The homogenate was collected, layered onto a 42% sucrose solution, and spun in a Beckman SW28 swinging bucket rotor at 25 000 rpm for 1 h at 4 °C. The fraction at the buffer−sucrose interface was collected and diluted to a total volume of 15 mL in buffer A. The membrane fraction was collected by centrifugation in a Beckman 75Ti rotor (35 000 rpm at 4 °C for 1 h). The pellet was resuspended in 10 mM PIPES/Tris, 2 mM EGTA, and 2 mM EDTA (pH 7.0) by homogenization with a 2 mL Teflon homogenizer (Wheaton). The total protein concentration was determined by the modified Lowry protein assay using Modified Lowry Protein

Table 1: Effect of Mutations in M5, -6, and -8 and the M5−6 and M7−8 Loops on the SCH28080 Affinity of the H,K-ATPase

location	mutant	K_i(SCH28080) ± SE (nM)	type of inhibition	V_{max} ± SE (μmol mg^{-1} h^{-1})	$K_{m,app}(NH_4^+)$ ± SE (mM)	H,K-ATPase (% of total protein)	$V_{max}/K_{m,app}(NH_4^+)$ ± SE
M5	P798C	163 ± 27	competitive	88.0 ± 3.6	2.4 ± 0.20	8.0	36.1 ± 4.4
	Y799F	90 ± 19	competitive	43.3 ± 2.1	1.2 ± 0.30	5.1	36.1 ± 10.8
	Y802F	65 ± 23	competitive	33.0 ± 2.8	1.0 ± 0.20	3.5	33.0 ± 9.4
	Y802L	125 ± 10	competitive	48.4 ± 1.4	0.6 ± 0.07	12.5	79.2 ± 11.9
	I803L	79 ± 11	competitive	40.8 ± 0.6	0.7 ± 0.06	10.0	57.8 ± 5.6
	S806N	102 ± 8	competitive	28.9 ± 1.3	2.2 ± 0.06	8.0	13.1 ± 0.9
M5−6 loop	V807I	96 ± 12	competitive	45.9 ± 4.5	1.3 ± 0.44	9.8	35.0 ± 15.3
	L809F	6150 ± 210	noncompetitive	39.0 ± 1.3	1.9 ± 0.30	3.0	20.5 ± 3.9
	L809V	288 ± 52	noncompetitive	85.0 ± 2.3	2.2 ± 0.17	8.4	38.3 ± 4.0
	P810A	281 ± 16	competitive	87.0 ± 2.1	2.2 ± 0.20	12.0	39.3 ± 4.5
	P810G	563 ± 17	competitive	108.5 ± 2.5	2.4 ± 0.24	11.0	44.7 ± 5.4
	L811F	625 ± 63	mixed	113.0 ± 1.9	2.0 ± 0.12	2.5	56.5 ± 4.3
	L811V	95 ± 26	competitive	80.9 ± 1.4	2.8 ± 0.17	9.6	29.4 ± 2.3
M6	C813A	182 ± 18	competitive	150.0 ± 3.5	5.5 ± 0.47	11.4	27.3 ± 3.0
	C813S	169 ± 30	competitive	62.9 ± 4.1	4.9 ± 0.96	9.0	12.8 ± 3.3
	C813T[a]	586 ± 69	competitive	40.0 ± 4.9	6.6 ± 1.80	0.4	6.1 ± 2.4
	I814F	249 ± 36	competitive	35.0 ± 0.8	0.4 ± 0.05	10.0	79.5 ± 10.9
	I814V	198 ± 51	competitive	56.0 ± 0.7	1.0 ± 0.05	9.0	56.0 ± 3.5
	I816L	309 ± 24	noncompetitive	30.5 ± 1.9	1.4 ± 0.36	6.0	21.7 ± 7.0
	F818C	265 ± 79	competitive	50.0 ± 1.8	1.8 ± 0.11	2.3	28.4 ± 2.8
	I819L	28 ± 12	mixed	48.8 ± 1.2	1.2 ± 0.11	2.0	40.0 ± 4.4
	T823V	133 ± 19	competitive	35.9 ± 0.6	0.8 ± 0.06	6.3	45.4 ± 4.2
M7−8 loop	Q905N	63 ± 11	competitive	30.3 ± 2.0	3.0 ± 0.30	4.5	10.2 ± 1.7
	E914Q	141 ± 42	competitive	31.4 ± 1.3	1.4 ± 0.23	12.0	22.0 ± 4.5
	F917Y	182 ± 63	competitive	74.9 ± 1.5	0.9 ± 0.08	3.2	79.9 ± 8.1
	G918E	151 ± 42	competitive	42.0 ± 2.1	2.4 ± 0.44	10.0	17.8 ± 4.2
	L921K			0.0		4.5	
M8	Y922I	151 ± 32	mixed	69.1 ± 4.2	1.5 ± 0.19	4.0	47.2 ± 8.9
	Q923V	65 ± 32	mixed	82.4 ± 4.0	1.3 ± 0.11	2.0	63.4 ± 8.3
	Q924E	66 ± 5	competitive	95.2 ± 2.6	1.6 ± 0.17	12.2	58.4 ± 7.7
	Y925A	82 ± 6	mixed	112.0 ± 3.7	2.3 ± 0.26	8.3	49.3 ± 7.3
	Y925F	372 ± 62	noncompetitive	30.6 ± 0.9	1.6 ± 0.16	4.6	19.1 ± 2.5
	Y928H	83 ± 16	competitive	56.7 ± 1.5	1.4 ± 0.05	5.5	42.0 ± 2.7
	T929L	512 ± 69	competitive	26.6 ± 1.0	1.2 ± 0.20	3.0	22.6 ± 4.7
	F932L	200 ± 72	competitive	132.0 ± 5.4	2.0 ± 0.28	2.0	66.7 ± 12.2
	M937V	281 ± 26	noncompetitive	42.8 ± 2.6	1.7 ± 0.40	2.1	24.9 ± 7.3
	I940A	248 ± 49	mixed	31.0 ± 0.7	1.4 ± 0.13	6.3	22.4 ± 2.6
	wt	64 ± 11	competitive	132.0 ± 3.2	2.4 ± 0.05	8.0	55.0 ± 1.3

[a] Data from ref *15*.

Assay Reagent (Pierce). The typical protein concentration was 5−10 μg/μL. The membranes were aliquoted, flash-frozen, and stored at −80 °C.

SDS−PAGE and Western Blot Analysis. Thirty microliters of gel sample buffer [4% SDS, 0.05% (w/v) bromophenol blue, 20% glycerol, and 1% (v/v) β-mercaptoethanol in 0.1 M Tris buffer (pH 6.8)] containing the membrane fractions (1−15 μg of protein) was loaded on a 7% SDS−polyacrylamide gel. As a standard for native α and β subunits, 40−170 ng of purified gastric vesicles (G1 fraction) (*21*) was used. Molecular weight standards (Bio-Rad Laboratories, Hercules, CA) were loaded on each gel.

After SDS−PAGE, proteins were transferred to nitrocellulose membranes (BioPlot-NC, Costar, Cambridge, MA). Membranes were washed twice with TBS [10 mM Tris, 150 mM NaCl, and 0.05% (v/v) Tween] and incubated in TBS containing 1% (w/v) bovine serum albumin. After 30 min, the membranes were incubated in the primary antibody solution (monoclonal antibody 12.18 against amino acids 666−689 of the α subunit of the H,K-ATPase, diluted 1:10000 in TBS, or monoclonal antibody 2B6 against amino acids 236−281 of the β subunit of the H,K-ATPase, diluted 1:1000 in TBS). After 1 h, membranes were washed twice with TBS and incubated with the secondary antibody solution [anti-mouse IgG conjugated to alkaline phosphatase (Promega, Madison, WI), diluted 1:2000 in TBS]. Then, after 1 h, membranes were washed twice and incubated for 15 min in TBS. After a final wash, the membranes were incubated for 5 min in AP buffer [100 mM Tris, 100 mM NaCl, and 5 mM $MgCl_2$ (pH 9.5)] containing a 0.3% (v/v) nitro blue tetrazolium solution and a 0.15% (v/v) 5-bromo-4-chloro-3-indolyl-1-phosphate solution according to the manufacturer's instructions (Promega).

Quantification of the Expressed H,K-ATPase. The content of the H,K-ATPase in the membrane fraction of the HEK293 cells was quantified by using purified hog gastric vesicles containing ≈85% H,K-ATPase (G1) (*21*) as a standard. Three different amounts of the membrane fraction and three different amounts of G1 were loaded on the same gel. SDS−PAGE and Western blot analysis with antibody 12.18 were performed as described above. All blots were scanned using the AMBIS optical imaging system (AMBIS Inc., San Diego, CA), and the optical density of the bands was measured; 40−170 ng of purified G1 yielded a linear calibration curve. For each membrane preparation, a range of loaded amounts of the membrane fraction giving values for the optical density similar to the densities obtained for G1 was chosen. The amount of the α subunit of the H,K-ATPase in the sample

was calculated using the calibration curve for G1. This allowed determination of the content of H,K-ATPase in crude membranes as the percentage of total membrane protein. The level of expression for each membrane preparation was calculated as the average of values obtained for three samples of the respective membrane fraction.

NH_4^+ Stimulated ATPase Activity. Na^+-free reaction buffer [40 mM Tris-HCl (pH 7.4), 2 mM $MgCl_2$ containing 1 mM EGTA (Ca-ATPases), 500 μM ouabain (Na,K-ATPase), 1 μM oligomycin (mitochondrial ATPase), 10 nM bafilomycin (V-type ATPases), and 100 nM thapsigargin (SERCA-ATPase) to suppress the activities of possible contaminating ATPases] in a total volume 75 μL contained 1−3 μL of a membrane fraction, various concentrations of NH_4Cl (0−40 mM), and 800 μM ATP. The reaction was terminated after 1 h at 37 °C by adding 100 μL of stop solution containing 0.046% (w/v) malachite green, 1.43% (w/v) ammonium molybdate, 1.36 N HCl, and 1.26% (v/v) NP-10. After 1 min, 25 μL of 34% sodium citrate was added. After 30 min, the absorbance at 680 nm was measured in a plate reader. Ion-stimulated ATPase activity was calculated as the difference between the extent of P_i release in the presence and absence of NH_4Cl. The activity was expressed in micromoles of P_i per milligram of total protein per hour and then converted to specific H,K-ATPase activity (micromoles of P_i per milligram of H,K-ATPase per hour) relative to a purified gastric vesicle preparation (G1) using the values for the content of expressed H,K-ATPase calculated from the quantitative Western blot analysis (see above).

Determination of V_{max}, $K_{m,app}(NH_4^+)$, and K_i(SCH28080). Data for the specific H,K-ATPase activities at various NH_4Cl concentrations (21−36 points) in the absence of inhibitor or at fixed concentration of inhibitor were fitted by nonlinear regression to the Michaelis−Menten equation (Enzfitter, BIOSOFT, 1999), and the $V_{max} \pm$ SE and the apparent K_m ($K_{m,app}$) ± SE for NH_4^+ were obtained. Each set of data points was plotted as an inverse plot to determine the mechanism of SCH28080 inhibition (competitive, noncompetitive, or mixed). The $K_i \pm$ SE was obtained from linear regression of the $K_{m,app}/V_{max}$ values plotted versus inhibitor concentration. The intersection of the linear regression with the *x*-axis gives the negative K_i.

Computer Representation. The visual interpretation of mutation results presented here is based on the assumption that the side chains of the H,K-ATPase are located in three-dimensional space in positions homologous to those in PDB entry 1kju that align with them in the Ca-ATPase sequence, and these alignments are shown in Figure 4A. This assumption is supported by homology in the ion binding residues of the transport site in M5 and M6, by homology of side chains within the M5−6 loop (notably, Pro784 and Leu787), the similar sequences in M8 between the H,K- and Ca-ATPase (ISIEMCQ and VTIEMCN, respectively), and the conserved number of residues in the M5−6 and M8 regions between the pumps which allows direct mapping of the H,K-ATPase residues onto the backbone of the Ca-ATPase structure without the need for modification of the backbone since we do not have to incorporate a different number of residues in the region where mutations affect either SCH28080 affinity or the nature of the inhibition.

There are side chain substitutions giving significantly different ranges of allowed ϕ and ψ angles in the M5−6 loop of the H,K-ATPase compared to those of the Ca-ATPase. To account for these differences, the side chains of the H,K-ATPase S^{806}VPLPLGC sequence were exchanged for those of the M5−6 loop of PDB entry 1kju (G^{782}-LPEALIP), the model of the E_2 form of the Ca-ATPase, and energy minimization was performed to a final average absolute derivative of <0.1 kcal mol^{-1} $Å^{-1}$ while keeping the N and A domains of the cytoplasmic domain fixed. This resulted in only a small change in the position of the backbone atoms of the M5−6 loop (rms deviation of 0.61 Å). This modified structure is illustrated in Figure 4B.

RESULTS

To evaluate the effect of mutations on ion affinity, we used the $V_{max}/K_{m,app}(NH_4^+)$ ratio that reflects the ability of the enzyme to interact with ion (*14*). Most of the mutations introduced here either did not change ion affinity or decreased it by ∼2−3-fold compared to that of the wild-type enzyme (Table 1). Three mutants (S806N, C813S, and Q905E) resulted in a 4−5-fold decrease in ion affinity, and C813T reduced ion affinity 9-fold.

The effect of mutations on SCH28080 affinity was found by plotting the $K_{m,app}/V_{max}$ values against inhibitor concentration which gives the negative K_i values for SCH28080. The effect of mutations will be discussed in relation to the structure of Figure 4B in terms of membrane helices M5, -6, and -8 and the loops between M5 and M6 and between M7 and M8.

Mutations in M5. Most of the mutations in M5, namely, Y799F, Y802F, I803L, and S806N, resulted in no change in either the inhibitor affinity or the mode of inhibition (Table 1). The NH_4^+-competitive inhibition kinetics for I803L are shown in Figure 1, which are similar to the kinetics of the wt enzyme, but the $K_{m,app}(NH_4^+)$ is increased without an effect on the V_{max}. The mutants P798C and Y802L displayed a 2−3-fold reduction in SCH28080 affinity with retention of the purely competitive character of SCH28080 inhibition (Table 1).

Mutations in the M5−6 Loop. Two mutations in the M5−6 loop, V807I and L811V, had no effect on inhibitor affinity or the type of inhibition (Table 1). On the other hand, mutation of P810 to G or A resulted in a 9- or 4-fold loss of SCH28080 affinity without a change in inhibition kinetics.

The L809F mutation not only resulted in a 96-fold loss of SCH28080 affinity but also changed the inhibition kinetics from competitive to noncompetitive (Table 1 and Figure 2). With the change of L809 to F, the inhibitor reduced the V_{max} but had no effect on the K_m for NH_4^+. The mutation of the same residue to a valine also resulted in noncompetitive kinetics but with an only 4-fold reduction in SCH28080 affinity. The L811F mutation resulted in a 10-fold decrease in SCH28080 affinity and mixed inhibition (Table 1).

Mutations in M6. Most of the mutations in M6, namely, C813A, C813S, I814F, I814V, F818C, and T823V, resulted in a 2−5-fold decrease in SCH28080 affinity, and cation-competitive kinetics were retained. In particular, the C813A and C813S substitutions reduced affinity 3-fold and the C813T substitution reduced inhibitor affinity 9-fold. In contrast, the I819L mutation displayed slightly higher inhibitor affinity but changed the character of inhibition from competitive to mixed (Table 1). Further, the I816L mutation

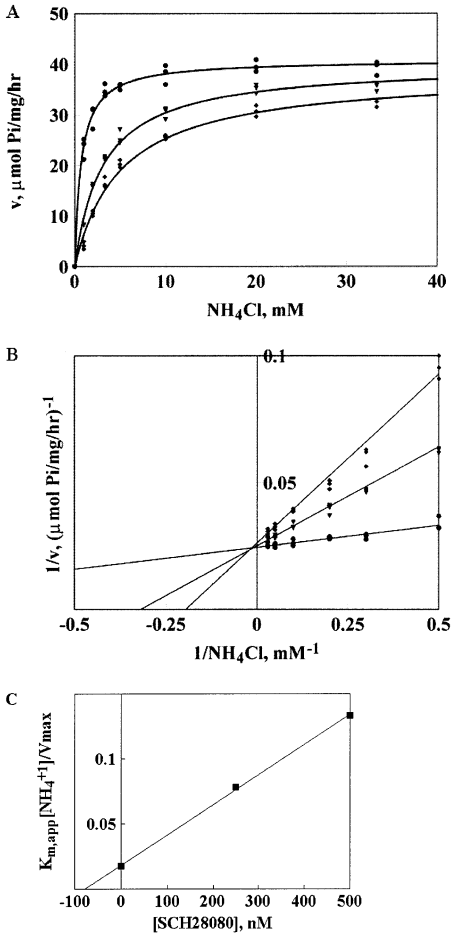

FIGURE 1: NH_4^+-competitive inhibition of the I803L mutant H,K-ATPase by SCH28080. (A) Michaelis−Menten plot. (B) Inverse plot of $1/v$ vs $1/[NH_4Cl]$. The lines intersect on the *y*-axis. (C) K_m/V_{max} replot. The points are K_m/V_{max} (the slopes of the inverse plot) vs the SCH28080 concentration. SCH28080 does not affect V_{max} and increases $K_{m,app}(NH_4^+)$. The intersection with the *x*-axis of the linear regression of these points shows the negative K_i(SCH28080) = 78.7 ± 11.5 nM: (●) no SCH28080 (V_{max} = 40.7 ± 0.6, K_m = 0.7 ± 0.1), (▼) 250 nM SCH28080 (V_{max} = 39.9 ± 0.9, K_m = 3.1 ± 0.2), and (◆) 500 nM SCH28080 (V_{max} = 38.2 ± 1.2, K_m = 5.1 ± 0.5).

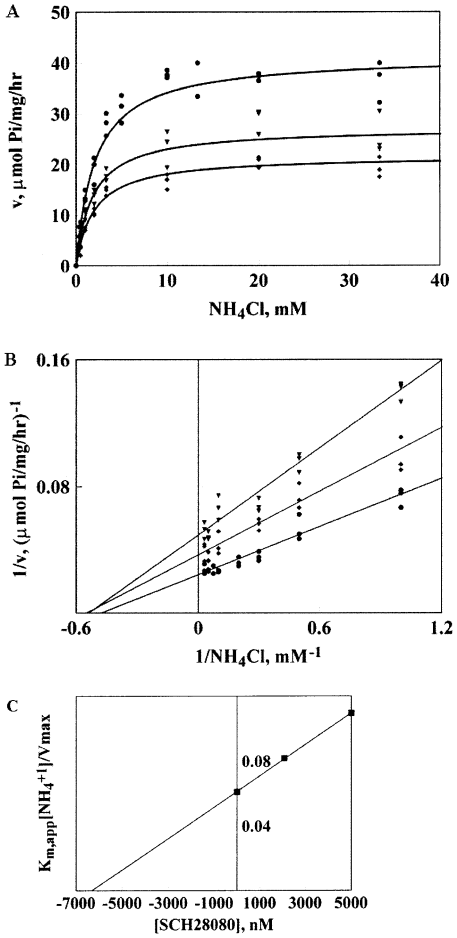

FIGURE 2: NH_4^+-noncompetitive inhibition of the L809F mutant H,K-ATPase by SCH28080. (A) Michaelis−Menten plot. (B) Inverse plot of $1/v$ vs $1/[NH_4Cl]$. SCH28080 reduces V_{max} and does not affect $K_{m,app}(NH_4^+)$. The lines intersect on the *x*-axis. (C) K_m/V_{max} replot. The points are K_m/V_{max} (the slopes of the inverse plot) vs the SCH28080 concentration. The intersection with the *x*-axis of the linear regression of these points shows the negative K_i(SCH28080) = 6315.8 ± 141.8 nM: (●) no SCH28080 (V_{max} = 41.2 ± 1.5, K_m = 2.1 ± 0.3), (▼) 2080 nM SCH28080 (V_{max} = 27.2 ± 1.5, K_m = 1.82 ± 0.5), and (◆) 5000 nM SCH28080 (V_{max} = 21.6 ± 0.7, K_m = 1.9 ± 0.2).

resulted in 5-fold loss in inhibitor affinity and noncompetitive inhibition kinetics.

Mutations in the M7−8 Loop. None of the mutations in the M7−8 loop changed the mode of SCH28080 inhibition. Q905N did not affect the inhibitor affinity, while E914Q, F917Y, and G918E resulted in a 2−3-fold decrease in affinity (Table 1).

Mutations in M8. In M8, only Q924E and Y928H resulted in no change in either inhibitor affinity or kinetics (Table 1). Q923V and Y925A had no effect on inhibitor affinity but resulted in mixed inhibition kinetics. The inhibitor increased the value of $K_{m,app}(NH_4^+)$ and reduced the V_{max} as shown for Y925A (Figure 3). The mutants T929L and F932L retained competitive inhibition but displayed 8- and 3-fold reduced inhibitor affinity, respectively. I940A reduced inhibitor affinity 4-fold but also resulted in mixed inhibition. The mutants Y925F and M937V resulted in 6- and 4-fold losses in SCH28080 affinity, respectively, and resulted in noncompetitive kinetics. The L921K mutation resulted in a complete loss of ion-stimulated activity.

DISCUSSION

The data discussed above are illustrated in Figure 4B. This illustration of the membrane domain of the H,K-ATPase is based on the structure of Ca-ATPase in the E_2 conformation (PDB entry 1kju). Although this P_2-type ATPase is only ~20% homologous to the H,K-ATPase or Na,K-ATPase, the structure of this region seems to be generally conserved among these three pumps as shown by a large number of mutagenesis studies that defined their ion binding residues (*22*−*28*).

Figure 4B shows that the mutations significantly reducing SCH28080 affinity are located on one side of the M5−6 loop region and at the luminal end of M6 and M8 (red and yellow), while mutations affecting ion binding are concentrated more toward the center of the membrane domain (blue).

Ion Transport Site Mutations. Mutations around the ion transport site near the middle of the membrane reduce ion affinity with a lesser effect on inhibitor affinity (*14*). The mutations E343Q, E820D, D824E, E936Q, and E936D result

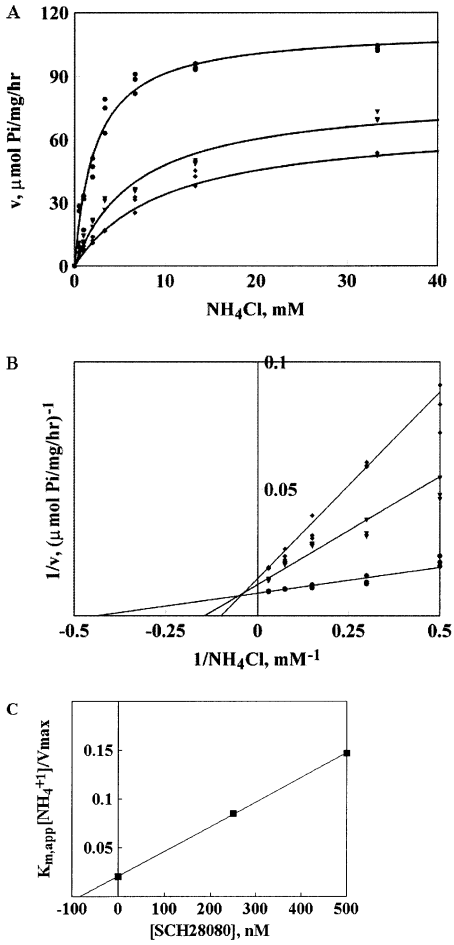

FIGURE 3: Mixed inhibition of the Y925A mutant H,K-ATPase by SCH28080. (A) Michaelis−Menten plot. (B) Inverse plot of $1/v$ vs $1/[NH_4Cl]$. SCH28080 reduces V_{max} and increases $K_{m,app}(NH_4^+)$. The lines intersect in the upper left quadrant. (C) K_m/V_{max} replot. The points are K_m/V_{max} (the slopes of the inverse plot) vs the SCH28080 concentration. The intersection with the *x*-axis of the linear regression of these points shows the negative K_i(SCH28080) = 82.1 ± 5.8 nM: (●) no SCH28080 (V_{max} = 112.0 ± 3.7, K_m = 2.3 ± 0.3), (▼) 250 nM SCH28080 (V_{max} = 81.1 ± 3.5, K_m = 6.9 ± 0.8), and (◆) 500 nM SCH28080 (V_{max} = 68.1 ± 3.6, K_m = 10.0 ± 0.9).

in a 2−3-fold decrease in inhibitor affinity and a 4−50-fold decrease in ion affinity (*14*). Although two mutations in the ion binding region, K791S and E795D, reduce SCH28080 affinity by 20- and 11-fold, respectively (*14*), they decrease ion affinity to a greater extent, by 54- and 63-fold, respectively. Further, there is no space with sufficient volume for the inhibitor adjacent to these residues, and the effect of their mutation on SCH28080 affinity is likely to be secondary to an effect on the structure of the ion binding site itself.

Mutations in the M5−6 Loop Region. In contrast, the mutations discussed here resulted in a loss of inhibitor affinity with either no effect or a lesser effect on ion affinity. The 96- and 4-fold reduction in inhibitor affinity in the L809F and L809V mutants, without a significant change in ion affinity (2.4- and 1.4-fold, respectively), suggests the direct involvement of this region in SCH28080 binding. The more significant impairment of binding in the phenylalanine as opposed to the valine mutation can be explained by the increased volume of phenylalanine as compared to that of valine or the wild-type residue, leucine. Whereas the valine side chain would give a loss of van der Waals contact with

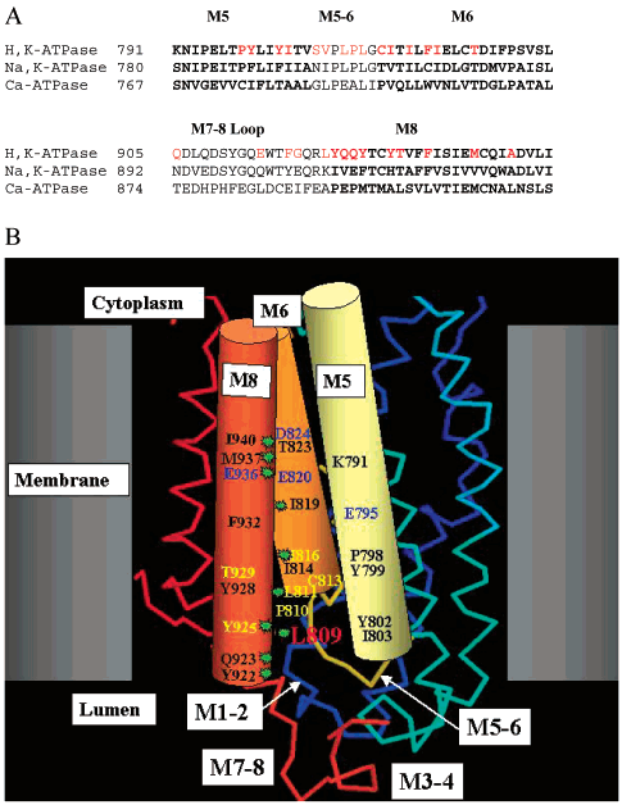

FIGURE 4: Representations of the binding site for SCH28080. (A) Alignment of the H,K-ATPase, Na,K-ATPase, and Ca-ATPase in the luminal regions of M5, M6, M8, and the M5−6 and M7−8 loops. The residues of the membrane helices are shown in bold, and the mutated residues are shown in red. (B) Illustration of the M5, M6, and M8 membrane and the M5−6 loop region of the gastric H,K-ATPase based on the Ca-ATPase in the E_2 conformation (PDB entry 1kju). The locations of the amino acids of the H,K-ATPase corresponding to the residues of the Ca-ATPase in M5, M6, M8, and the M5−6 loop are shown based on the alignment shown in panel A. This depicts the residues whose mutations resulted in a significant decrease in SCH28080 affinity (red for 100-fold and yellow for 5−9-fold) and noncompetitive or mixed inhibition kinetics (green stars). Ion binding residues defined by mutagenesis are shown in blue. It can be seen that the residues affecting affinity are clustered in an apparent vestibule close to the luminal surface of the enzyme, distal to the ion binding site, and that the mutations altering kinetics are on adjacent surfaces of M6 and M8.

the inhibitor and a modest effect on binding, the phenyl side chain is likely to occupy some of the space required for normal interaction of the inhibitor with the wild-type enzyme and thereby decrease the binding affinity more significantly, as was found.

Substitution of the adjacent residue, P810G or -A, resulted in a 10- or 4-fold lower SCH28080 sensitivity, respectively (Table 1). This could be due to the involvement of this proline side chain in inhibitor binding or a conformational change in the M5−6 loop that affects the position of the L809 side chain.

The direct contribution of L809 to SCH28080 binding is in agreement with recently published data on the involvement of C813 at the end of the M5−6 loop in the inhibitor site (*15*). The proximity of L809 to C813 at the luminal end of M6 suggests both residues make contributions to SCH28080 binding. The mutation of Cys813 to the threonine present in SCH28080 that is insensitive Na,K-ATPase resulted in a 9-fold loss in inhibitor affinity (*15*), and even conservative

mutations to a serine and a smaller alanine resulted in a 3-fold decrease in affinity (Table 1). This cysteine also forms a disulfide bond with covalent proton pump inhibitors such as omeprazole, accounting for their inhibition of acid secretion (*29*) and demonstrating the presence of a space adjacent to C813 with sufficient volume to bind SCH28080. Antagonism between SCH28080 and omeprazole in inhibition of acid transport further suggested the binding sites of the two classes of inhibitors might overlap (*30*). This is in agreement with the postulated binding of SCH28080 between L809 and C813.

Although mutation of L811 to F significantly reduced the extent of SCH28080 binding, substitution with a smaller side chain, valine, did not alter the inhibitor affinity (Table 1). The presence of a proline between L809 and L811 suggests that the side chains of L809 and L811 in the M5−6 loop face in opposite directions. The side chain of L811 therefore is unlikely to interact with the inhibitor directly. Replacement of the leucine side chain with the bulkier phenyl group is likely to displace the M5−6 loop into the binding space to reduce inhibitor affinity. This effect would not be given by valine, the side chain of which is smaller than that of leucine.

Mutations in M6 and M8. The mutation of I816 to leucine near the luminal end of M6 and close to L809 and C813 resulted in a 5-fold reduction in SCH28080 affinity, in agreement with previously published data where the I816A mutant also resulted in a decreased SCH28080 affinity (*16*), suggesting a direct or indirect contribution of this residue to inhibitor binding.

The acquisition of some SCH28080 sensitivity by the chimera containing the Q905−V930 sequence of the gastric H,K-ATPase placed into the Na,K-ATPase (*31*) suggested the involvement of the M7−8 loop and/or the luminal end of M8 in SCH28080 binding. The mutation of the residues that are not conserved between H,K-ATPase and Na,K-ATPase in the Q905−V930 fragment of the H,K-ATPase to the corresponding Na,K-ATPase residues resulted in no change or a slight change in inhibitor affinity (Table 1) for most of the mutants but in 6- and 8-fold losses in SCH28080 affinity in the Y925F and T929L mutants, respectively. The proximity of E785 aligned with L809 in PDB entry 1kju to the Ca-ATPase residues that correspond to Y925 (4.8 Å) and T929 (7.6 Å) might suggest a direct contribution of Y925 and T929 to inhibitor binding. The proximity of the para position of the phenyl group in bound SCH28080 to some part of the sector enclosing M1 and M2 is also required since a photoaffinity derivative of SCH28080, Me-DAZIP$^+$ (*32*), labels within this region in a K^+-competitive manner. On the basis of the structure of PDB entry 1kju, the luminal end of M2 near L141 is the most likely choice (the distance between the Ca-ATPase residues that correspond to L809 and L141 is 10.8 Å). Considering the dimensions of SCH28080 (11 Å × 16 Å) and the distances between the corresponding residues in the structure of PDB entry 1kju, we suggest that the SCH28080 binding region in the space adjacent to L809 and C813 could include a surface contributed by Y925 and T929 on one side and a portion of the M4 surface near M334 (*17*) on the other with the phenyl ring projecting toward M2 near L141. An alternate explanation would have both T929 and Y925 contributing indirectly to SCH28080 binding affinity by affecting the conformation of the M5−6 loop. Similarly, I816 might affect the position of C813 and L809.

Residues Affecting Competitive Kinetics. Several mutations resulted in noncompetitive or mixed SCH28080 inhibition kinetics (Table 1 and Figure 4B). These mutations did not affect the ion affinity, indicating they did not affect the ion site, and I819L, Q923V, and Y925A reduced neither ion nor inhibitor affinity. The simplest explanation is a change in the accessibility of the cation to the binding domain in the presence of bound inhibitor in these mutants. These mutations are placed on the opposing faces of the M6 and M8 helices, as illustrated with green stars in Figure 4B. Each of the I819L, I816L, Y922I, Q923V, I940A, M937V, E936D, Y925F, and Y925A mutations could alter the spacing between M6 and M8 that then could allow ion access to the transport sites in the middle of the membrane despite the presence of the inhibitor on the enzyme bound in the luminal vestibule. Hence, these mutations appear to modify the normal ion pathway or, perhaps, create an alternate ion pathway.

In summary, the illustration in Figure 4B suggests that the SCH28080 binding region contains the surface between L809 in the M5−6 loop and C813 at the luminal end of M6, approximately two helical turns distal to the ion transport site, where it blocks the luminal ion access pathway. This representation is compatible with previously published results concerning mutations lowering SCH28080 affinity in M4 [M334I (*17*)] and M6 [I816A (*16*)] and is also compatible with previously published data on a possible contribution of the Q905−V930 region to SCH28080 binding (*31*). The postulated region of binding of SCH28080 also allows interaction of the inhibitor with the M1-M2 region as previously found by photoaffinity labeling (*32*). Further, the binding site illustrated here predicts an overlap between the imidazopyridine binding site and the covalent binding site of omeprazole, explaining the reduction in the extent of omeprazole inhibition caused by the presence of SCH28080 (*30*). The mutations that change inhibitor kinetics are on the adjacent faces of M6 and M8 and potentially can affect ion entry into the transport sites. The mutations in this region apparently modify the enzyme structure so that K^+ can access the ion transport site even with SCH28080 bound.

ACKNOWLEDGMENT

Primary antibodies mAb 12.18 and 2B6 against the H,K-ATPase α and β subunits were generous gifts from Dr. A. Smolka, and Dr. T. Masuda, respectively.

REFERENCES

1. Goldshleger, R., Tal, D. M., and Karlish, S. J. (1995) *Biochemistry 34*, 8668−8679.
2. Shin, J. M., Kajimura, M., Arguello, J. M., Kaplan, J. H., and Sachs, G. (1994) *J. Biol. Chem. 269*, 22533−22537.
3. Sachs, G., Shin, J. M., Besancon, M., Munson, K., and Hersey, S. (1992) *Ann. N.Y. Acad. Sci. 671*, 204−216.
4. Besancon, M., Shin, J. M., Mercier, F., Munson, K., Miller, M., Hersey, S., and Sachs, G. (1993) *Biochemistry 32*, 2345−2355.
5. Shin, J. M., Besancon, M., Bamberg, K., and Sachs, G. (1997) *Ann. N.Y. Acad. Sci. 834*, 65−76.
6. Lutsenko, S., and Kaplan, J. H. (1992) *Ann. N.Y. Acad. Sci. 671*, 147−155.
7. Sachs, G., Chang, H. H., Rabon, E., Schackman, R., Lewin, M., and Saccomani, G. (1976) *J. Biol. Chem. 251*, 7690−7698.
8. Yoda, A., and Yoda, S. (1975) *Mol. Pharmacol. 11*, 653−662.
9. Wallick, E. T., and Schwartz, A. (1988) *Methods Enzymol. 156*, 201−213.

10. Wallmark, B., Briving, C., Fryklund, J., Munson, K., Jackson, R., Mendlein, J., Rabon, E., and Sachs, G. (1987) *J. Biol. Chem. 262*, 2077−2084.
11. Mendlein, J., and Sachs, G. (1990) *J. Biol. Chem. 265*, 5030−5036.
12. Palasis, M., Kuntzweiler, T. A., Arguello, J. M., and Lingrel, J. B. (1996) *J. Biol. Chem. 271*, 14176−14182.
13. Toyoshima, C., Nakasako, M., Nomura, H., and Ogawa, H. (2000) *Nature 405*, 647−655.
14. Vagin, O., Munson, K., Lambrecht, N., Karlish, S. J., and Sachs, G. (2001) *Biochemistry 40*, 7480−7490.
15. Lambrecht, N., Munson, K., Vagin, O., and Sachs, G. (2000) *J. Biol. Chem. 275*, 4041−4048.
16. Asano, S., Matsuda, S., Hoshina, S., Sakamoto, S., and Takeguchi, N. (1999) *J. Biol. Chem. 274*, 6848−6854.
17. Munson, K. B., Lambrecht, N., and Sachs, G. (2000) *Biochemistry 39*, 2997−3004.
18. Bamberg, K., Mercier, F., Reuben, M. A., Kobayashi, Y., Munson, K. B., and Sachs, G. (1992) *Biochim. Biophys. Acta 1131*, 69−77.
19. Reuben, M. A., Lasater, L. S., and Sachs, G. (1990) *Proc. Natl. Acad. Sci. U.S.A. 87*, 6767−6771.
20. Lambrecht, N., Corbett, Z., Bayle, D., Karlish, S. J., and Sachs, G. (1998) *J. Biol. Chem. 273*, 13719−13728.
21. Rabon, E. C., Im, W. B., and Sachs, G. (1988) *Methods Enzymol. 157*, 649−654.
22. Nielsen, J. M., Pedersen, P. A., Karlish, S. J., and Jorgensen, P. L. (1998) *Biochemistry 37*, 1961−1968.
23. Rice, W. J., Green, N. M., and MacLennan, D. H. (1997) *J. Biol. Chem. 272*, 31412−31419.
24. Kuntzweiler, T. A., Wallick, E. T., Johnson, C. L., and Lingrel, J. B. (1995) *J. Biol. Chem. 270*, 2993−3000.
25. Jewell-Motz, E. A., and Lingrel, J. B. (1993) *Biochemistry 32*, 13523−13530.
26. Hermsen, H. P., Swarts, H. G., Koenderink, J. B., and De Pont, J. J. (1998) *Biochem. J. 331*, 465−472.
27. Asano, S., Tega, Y., Konishi, K., Fujioka, M., and Takeguchi, N. (1996) *J. Biol. Chem. 171*, 2740−2745.
28. Swarts, H. G., Klaassen, C. H., Boer, M. d., Fransen, J. A., and Pont, J. J. D. (1996) *J. Biol. Chem. 271*, 29764−29772.
29. Besancon, M., Simon, A., Sachs, G., and Shin, J. M. (1997) *J. Biol. Chem. 272*, 22438−22446.
30. Hersey, S. J., Steiner, L., Mendlein, J., Rabon, E., and Sachs, G. (1988) *Biochim. Biophys. Acta 956*, 49−57.
31. Farley, R. A., Schreiber, S., Wang, S. G., and Scheiner-Bobis, G. (2001) *J. Biol. Chem. 276*, 2608−2615.
32. Munson, K. B., Gutierrez, C., Balaji, V. N., Ramnarayan, K., and Sachs, G. (1991) *J. Biol. Chem. 266*, 18976−18988.

BI025921W